



Cite as
Nano-Micro Lett.
(2024) 16:202

Received: 2 January 2024
Accepted: 5 April 2024
© The Author(s) 2024

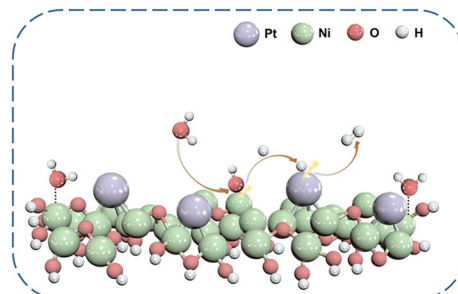
Achieving Negatively Charged Pt Single Atoms on Amorphous Ni(OH)₂ Nanosheets with Promoted Hydrogen Absorption in Hydrogen Evolution

Yue Liu^{1,2}, Gui Liu¹, Xiangyu Chen¹, Chuang Xue¹, Mingke Sun¹, Yifei Liu¹, Jianxin Kang¹ ✉, Xiujuan Sun² ✉, Lin Guo¹ ✉

HIGHLIGHTS

- Pt–Ni bonded Pt single-atom (SA) catalyst, rather than classic Pt–O bonded SA catalyst, was successfully constructed.
- The electronic states of Pt SA catalyst were deeply regulated and negatively charged Pt^{δ−} was realized.
- Pt–Ni bonded Pt SA catalyst-enhanced absorbability for activated hydrogen atoms and promoted hydrogen absorption.

ABSTRACT Single-atom (SA) catalysts with nearly 100% atom utilization have been widely employed in electrolysis for decades, due to the outperforming catalytic activity and selectivity. However, most of the reported SA catalysts are fixed through the strong bonding between the dispersed single metallic atoms with nonmetallic atoms of the substrates, which greatly limits the controllable regulation of electrocatalytic activity of SA catalysts. In this work, Pt–Ni bonded Pt SA catalyst with adjustable electronic states was successfully constructed through a controllable electrochemical reduction on the coordination unsaturated amorphous Ni(OH)₂ nanosheet arrays. Based on the X-ray absorption fine structure analysis and first-principles calculations, Pt SA was bonded with Ni sites of amorphous Ni(OH)₂, rather than conventional O sites, resulting in negatively charged Pt^{δ−}. In situ Raman spectroscopy revealed that the changed configuration and electronic states greatly enhanced absorbability for activated hydrogen atoms, which were the essential intermediate for alkaline hydrogen evolution reaction. The hydrogen spillover process was revealed from amorphous Ni(OH)₂ that effectively cleave the H–O–H bond of H₂O and produce H atom to the Pt SA sites, leading to a low overpotential of 48 mV in alkaline electrolyte at $-1000 \text{ mA cm}^{-2} \text{ mg}^{-1} \text{ Pt}$, evidently better than commercial Pt/C catalysts. This work provided new strategy for the controllable modulation of the local structure of SA catalysts and the systematic regulation of the electronic states.



KEYWORDS Hydrogen evolution reaction; Amorphous; Pt single atoms; Hydrogen spillover

Yue Liu, Gui Liu, and Xiangyu Chen have contributed equally to this work.

✉ Jianxin Kang, kangjianxin@buaa.edu.cn; Xiujuan Sun, sunxj594@xtu.edu.cn; Lin Guo, guolin@buaa.edu.cn

¹ School of Chemistry, Beijing Advanced Innovation Center for Biomedical Engineering, Key Laboratory of Bio-inspired Smart Interfacial Science and Technology, Beihang University, Beijing 100191, People's Republic of China

² School of Chemistry, Key Laboratory of Environmentally Friendly Chemistry and Applications of Ministry of Education, Xiangtan University, Xiangtan 411105, Hunan, People's Republic of China

Published online: 23 May 2024



SHANGHAI JIAO TONG UNIVERSITY PRESS

Springer

1 Introduction

Hydrogen evolution reaction (HER), as a half-reaction of water electrolysis, provides a practical way to produce hydrogen with excellent energy conversion efficiency, arousing great interest in the exploration and development of highly active catalysts [1–4]. Among all the catalysts, noble metal-based catalysts represented by Pt demonstrate excellent specific activity and selectivity, which are widely used in HER [5–7]. As the scarce reserves and expensive prices seriously limit their scaling up, single-atom (SA) catalysts with the maximum atomic utilization, afford an alternative for the application of noble metal-based catalysts [8–10]. However, in order to fix the metal atoms and prevent the agglomeration, most of the reported SA catalysts were strongly bonded with the nonmetal atoms (O, N, etc.) of the substrate [11–13]. It will inevitably lead to the oxidation of the metal atoms and further hinder the regulation of the electronic states, diminishing their electrocatalytic properties. For example, oxidized noble metal atoms would reduce the adsorption capacity for hydrogen atoms, limiting the HER activity of the catalysts [11].

Unlike widely used crystalline substrates, amorphous materials demonstrate advantages as substrates in optimizing the geometrical and electronic structure of SA due to their unique long-range disordered and isotropic structural features [14–19]. The disordered adjacent atoms on the amorphous substrates could geometrically change the active sites and rearrange the distribution of electrons, which may accelerate the charge transfer between active centers, and enhance the electrochemical activity of the active sites [11, 20, 21]. Meanwhile, the abundant dangling bonds and defects in the amorphous substrate can anchor the SA and effectively improve the structural stability of SA catalysts in long-term service [22–24]. The key point is that the highly coordination unsaturated local environment of exposed metal atoms on the surface of amorphous substrate could provide the possibility of constructing metal–metal bonding, instead of the conventional metal–nonmetal bonding for SA loading [7, 8, 25]. The novel structure could subversively modulate the electronic structure of the SA catalysts, further promoting the catalytic performance [20].

Here, we report a novel Pt SA catalyst fixed by Pt–Ni bonding on amorphous Ni(OH)₂ nanosheet arrays through a controllable electrochemical reduction strategy. The coordination unsaturated atomic structure of amorphous substrate provides sufficient sites for the adsorption of PtCl₆²⁻ ions,

while the nascent Pt SA from reduction is captured by the exposed Ni metal sites at the oxygen vacancies to form Pt–Ni bonds instead of the conventional Pt–O bonds. Both of the density functional theory (DFT) calculation and in situ Raman spectroscopy demonstrate the enhanced absorbability for activated hydrogen atoms, which facilitates hydrogen spillover processes between amorphous Ni(OH)₂ substrate and Pt SA in the alkaline. The amorphous Ni(OH)₂ substrate efficiently cleaves water molecules and delivers hydrogen atoms to the Pt sites, significantly increasing the hydrogen coverage on the Pt SA and leading to the enhanced HER performance. This work provides a method for the development of highly active SA catalysts, which could efficiently promote the hydrogen production in alkaline solution.

2 Experimental Section

2.1 Chemicals

Carbon fiber paper (TGP-H-060, Toray Industries, Japan), Ni(acac)₂·2H₂O (96%, J&K Scientific Inc., China), anisole (99%, Innochem Inc., China), Ni(OH)₂ (99%, J&K Scientific Inc., China), Pt/C (Pt 20%, Alfa Aesar Inc., USA), Nafion solution (5 wt% in water, J&K Scientific Inc., China), KOH (85%, Alfa Aesar Inc., USA), and chloroplatinic acid (H₂PtCl₆) (Pt ≥ 37.5%, Macklin, China).

2.2 Catalysts Preparation

2.2.1 Synthesis of Ni(acac)₂ Nanosheet Arrays

30 mg of Ni(acac)₂·2H₂O was placed in a 100 mL flask and 30 mL of anisole was added, followed by a water bath for 1 h to accelerate the dissolution of Ni(acac)₂·2H₂O. And then 1 × 2 cm² of carbon fiber paper (CFP) was added to the solution and the flask was moved into an oil bath at 120 °C for 2 h. After that, the CFP was taken out and washed with ethanol several times.

2.2.2 Synthesis of a-Ni(OH)₂ Nanosheet Arrays

The constant current activation method was used to transform Ni(acac)₂ nanosheet arrays into amorphous Ni(OH)₂ (a-Ni(OH)₂) nanosheet arrays by removing the

organic groups. In a two-electrode system, the as-prepared nanosheet arrays was employed as the anode and the constant current electrolysis was conducted under a constant current of 5 mA in a 1 M KOH solution for 5–6 h.

2.2.3 Synthesis of Pt-SA/a-Ni(OH)₂

Electroplating was used for the synthesis of single-atom Pt on the a-Ni(OH)₂ nanosheet arrays (Pt-SA/a-Ni(OH)₂). In a typical experiment, the a-Ni(OH)₂ was served as the cathode, together with a carbon rod as the counterpart electrode and Hg/HgO electrode as the reference electrode, and then placed in a 1 M KOH solution containing 10⁻⁵ M PtCl₆²⁻ solution. Constant voltage electrolysis was conducted at -0.079 V vs. RHE for 20 min, during which the platinum in the solution is reduced and plated onto the a-Ni(OH)₂ nanosheet arrays.

2.2.4 Synthesis of Pt-NP/a-Ni(OH)₂

The reference material was synthesis in a similar method with Pt-SA/a-Ni(OH)₂. For the synthesis of nanoparticle Pt on a-Ni(OH)₂ nanosheet arrays, the electroplating time was 40 min, with other parameters remaining the same in the synthesis of Pt-SA/a-Ni(OH)₂.

2.2.5 Preparation of Pt/C Catalyst

20 mg of commercial Pt/C (20 wt%) catalyst was dispersed in 990 μL of ethanol, followed by the addition of 10 μL of 5 wt% nafion solution. After 20 min of sonication, a homogeneous ink was obtained. Finally, 100 μL of ink was pipetted to the CFP (1 × 1 cm²) on both sides for even coating, and dried in air.

2.2.6 Preparation of Pt/CFP

The reference material was synthesized in a similar method with Pt-SA/a-Ni(OH)₂. For the synthesis of Pt on CFP (Pt/CFP), the substrate for electroplating was the bared carbon fiber paper. And the parameters of electroplating were the same with those in the synthesis of Pt-SA/a-Ni(OH)₂. In a typical experiment, the loading amount of Pt in Pt/CFP is tested to be 0.15%.

2.2.7 Synthesis of Pt-SA/commercial Ni(OH)₂

For the synthesis of single atom Pt on commercial Ni(OH)₂ (Pt-SA/commercial Ni(OH)₂), 5 mg of commercial Ni(OH)₂ was dispersed in 990 μL of ethanol, followed by the addition of 10 μL of nafion solution. The prepared Ni(OH)₂ ink was dropped onto a CFP (1 × 2 cm²). Next, this CFP was used as the working electrode and the electroplating of single atom Pt was conducted. The parameters of electroplating were the same with those in the synthesis of Pt-SA/a-Ni(OH)₂.

3 Results and Discussion

3.1 Morphology of Pt-SA/a-Ni(OH)₂

β-Ni(OH)₂ demonstrates a stratified structure connected by Ni-O₆ octahedrons as units, with hydroxyl groups facing outwards [26]. Thus, when it is employed as the substrate to construct SA catalysts, the loaded metal atoms can only be coordinated with oxygen atoms. In contrast, the amorphous Ni(OH)₂ presents a large number of unsaturated Ni sites with oxygen vacancies [27], which provide an ideal platform for the establishment of single metal atom bonding to Ni sites (Fig. 1a). The substrate was constructed in two steps. Firstly, Ni(acac)₂ nanosheet arrays were grown on carbon fibers (Fig. 1b); secondly, amorphous Ni(OH)₂ nanosheet arrays were generated through the electrochemical transformation from Ni(acac)₂ nanosheet arrays (Fig. 1c) [28]. Next, Pt SA was loaded on amorphous Ni(OH)₂ nanosheet arrays (named as Pt-SA/a-Ni(OH)₂) by electrochemical reduction in 10⁻⁵ M PtCl₆²⁻ solution at -0.079 V vs. RHE for 20 min (Fig. 1d). Transmission electron microscopy (TEM) results showed that amorphous Ni(OH)₂ nanosheets were grown vertically on carbon fibers (Fig. 1e-g), providing a large area for the deposition of Pt SA. Aberration corrected high-angle annular dark field (AC-HAADF) image showed that Ni(OH)₂ nanosheets have no obvious lattice fringes, evidencing an amorphous structure. The Pt SA as brighter spots are dispersedly loaded on amorphous Ni(OH)₂ nanosheets, without the appearance of Pt clusters or particles (Fig. 1h). The loading amount of Pt in Pt-SA/a-Ni(OH)₂ was calculated to be ~0.07 wt% through inductively coupled plasma optical emission spectrometer (ICP-OES) (Fig. S1). If the electrochemical

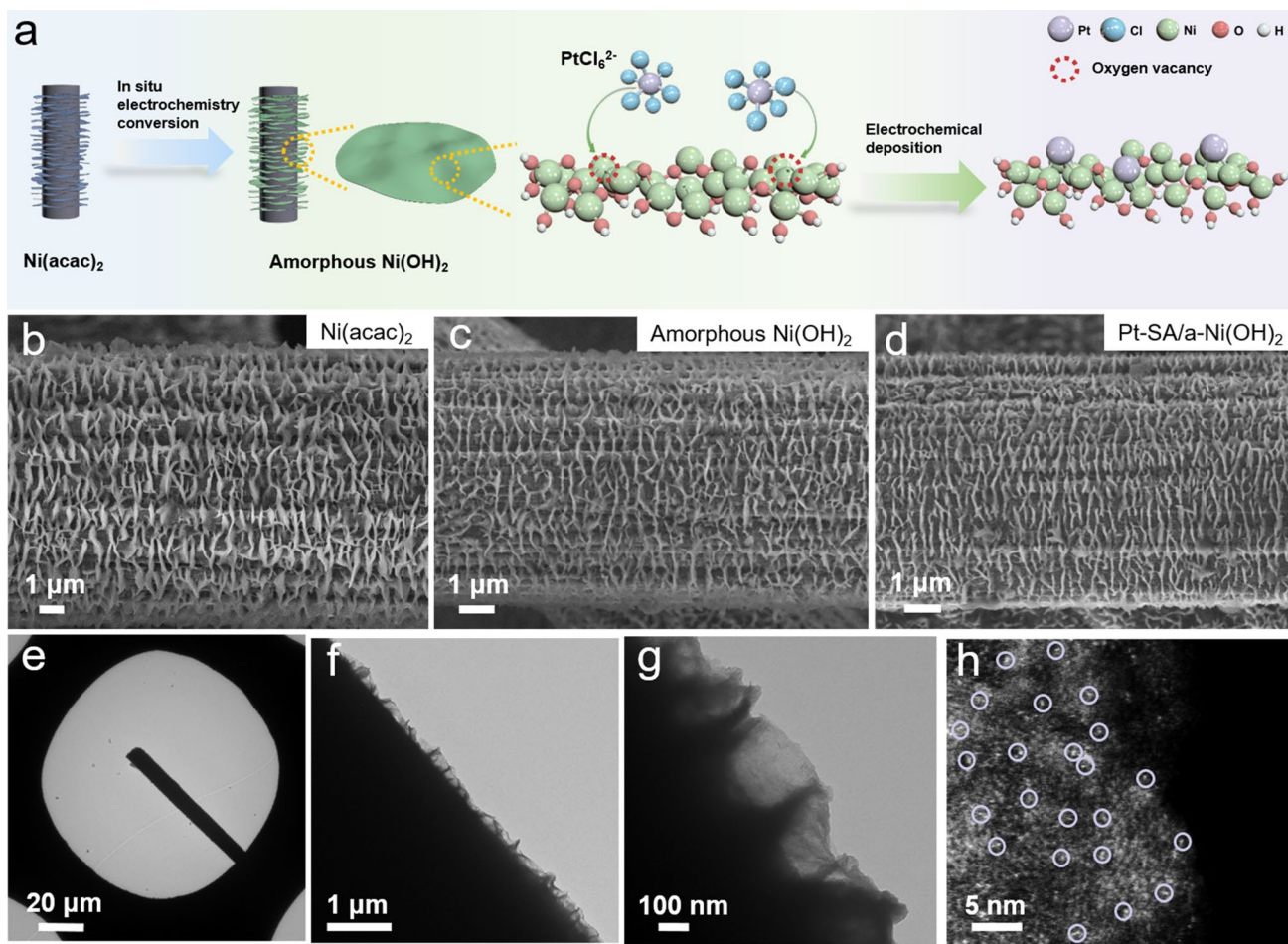


Fig. 1 Pt SA on amorphous Ni(OH)₂ nanosheet arrays. **a** Schematic diagram of Pt-SA/a-Ni(OH)₂ growth. **b-d** Scanning electron microscopy (SEM) images of Ni(acac)₂ nanosheet arrays, amorphous Ni(OH)₂ nanosheet arrays and Pt-SA/a-Ni(OH)₂ catalyst. **e-g** Step-by-step enlarged TEM images of Pt-SA/a-Ni(OH)₂ catalyst. **h** AC-HAADF image of Pt-SA/a-Ni(OH)₂ catalyst

reduction time was extended to more than 40 min, Pt nanoparticles (Pt-NP/a-Ni(OH)₂) were observed (Fig. S2), instead of single atom. The electron paramagnetic resonance (EPR) spectra of the amorphous Ni(OH)₂ nanosheets and the Pt-SA/a-Ni(OH)₂ catalyst exhibited typical signals at $g = 2.003$, confirming the existence of the oxygen vacancies in the system (Fig. S3). The presence of oxygen vacancies helps to stabilize Pt SA on the substrate.

3.2 Atomic Structure of Pt-SA/a-Ni(OH)₂

In order to demonstrate the atomic structure of the Pt-SA/a-Ni(OH)₂ catalyst, we then investigated the coordination

environment of Pt in Pt-SA/a-Ni(OH)₂ through X-ray absorption fine structure (XAFS) analysis (Fig. 2a). In the Fourier transformed extended X-ray absorption fine structure (EXAFS) spectra (Figs. 2b and S4, Table S1), the Pt foil exhibited a clear Pt-Pt bond at 2.5 Å, and the bond was almost unrecognizable in the Pt-SA/a-Ni(OH)₂ sample, confirming the single atom state of Pt [29–31]. At the same time, the main peak of Pt-SA/a-Ni(OH)₂ catalyst located at 2.3 Å was also distinguishing from Pt-O bond of standard Pt-O₂ at 1.6 Å [32, 33]. It meant that Pt-SA/a-Ni(OH)₂ catalyst displayed a different structure from the conventional SA materials based on Pt-O bonding, which we have also synthesized by employing commercially crystalline Ni(OH)₂ as a substrate (Fig. S5). It is interesting that the Pt signal in

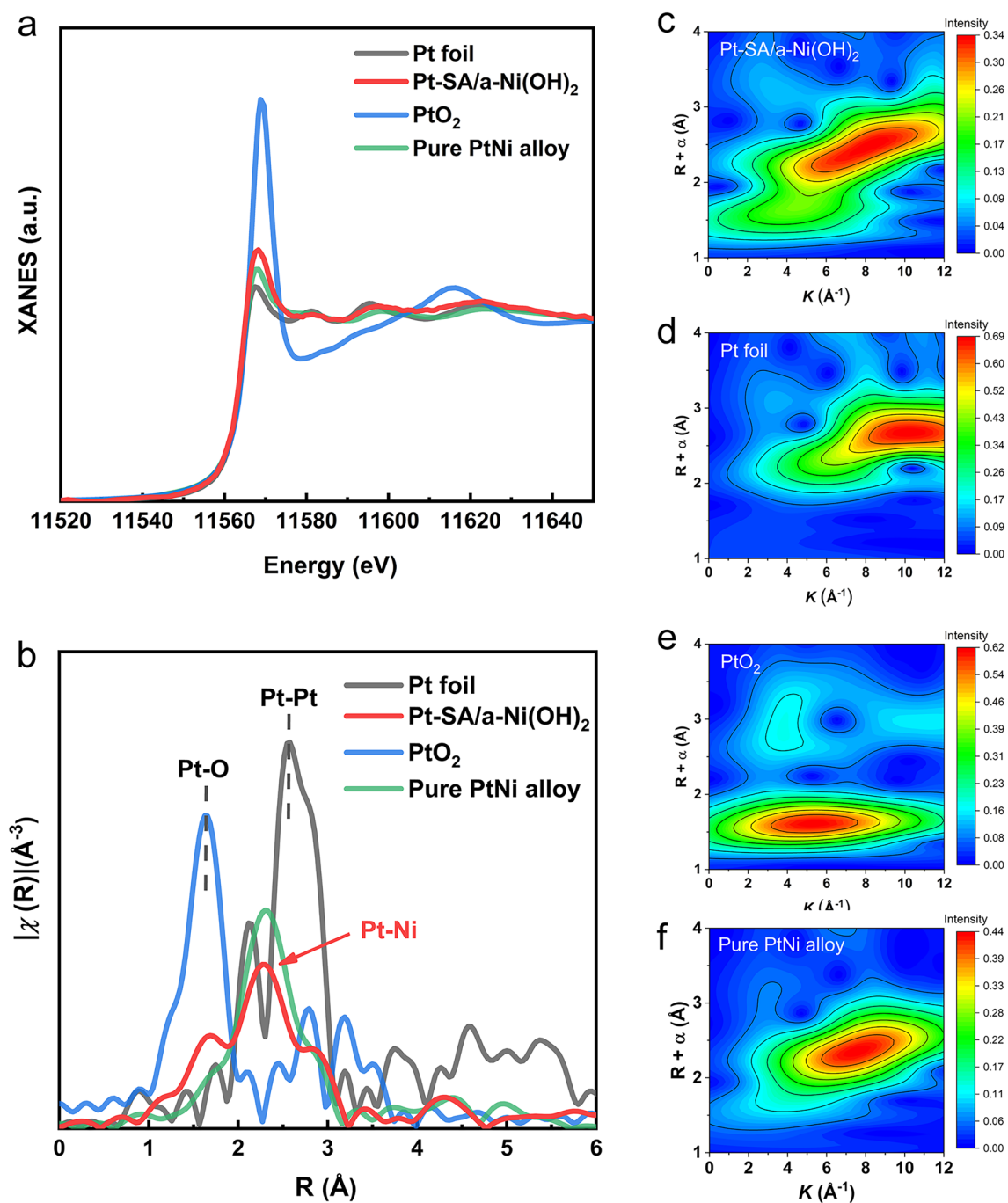


Fig. 2 Pt–Ni bonding in Pt–SA/a–Ni(OH)₂ catalyst. **a** Pt L_{3} -edge XAFS spectra of Pt–SA/a–Ni(OH)₂ catalyst, PtO₂, Pt foil and PtNi alloy. **b** Fourier transformed EXAFS spectra of Pt L_{3} -edge of Pt–SA/a–Ni(OH)₂ catalyst, PtO₂, Pt foil and PtNi alloy. **c–f** Wavelet transform EXAFS of **c** Pt–SA/a–Ni(OH)₂ catalyst, **d** Pt foil, **e** PtO₂, **f** PtNi alloy

Pt–SA/a–Ni(OH)₂ is basically the same as that of Pt in the Pt–Ni alloy, which proves the bond of Pt–Ni in Pt–SA/a–Ni(OH)₂ catalyst (Fig. S6). Similarly, the Pt–Ni bond can be directly observed as the dominant form of Pt present in this system through wavelet transformations [34], rather than the

Pt–Pt bond of bulk Pt or the Pt–O bond for conventional Pt SA materials (Fig. 2c–f).

To further verify Pt–Ni bonding in the catalyst, X-ray photoelectron spectroscopy (XPS) characterization was employed to perform series of supported Pt catalysts

with different loading forms from Pt SA to Pt nanoparticles, according to the electrodeposition time (20, 40, and 120 min). Two sets of Pt 4*f* peaks were present for Pt(0) and Pt(IV), with an additional Ni 3*p* peak for the Ni(OH)₂ substrate (Figs. 3a, b and S7). Taking the peak of Ni 3*p* as a reference, the positions of Pt(IV) peak in the catalysts

remained unchanged, while that of Pt(0) peak exhibited a regular shift. Interestingly, with the electrodeposition time increasing, the binding energies of Pt 4*f*_{7/2} and Pt 4*f*_{5/2} of Pt(0) gradually shifted to that of commercial Pt/C (Figs. 3c and S8). Thus, the Pt in Pt-SA/a-Ni(OH)₂ was negatively charged, denoted as Pt^{δ-}. It indicated that, for

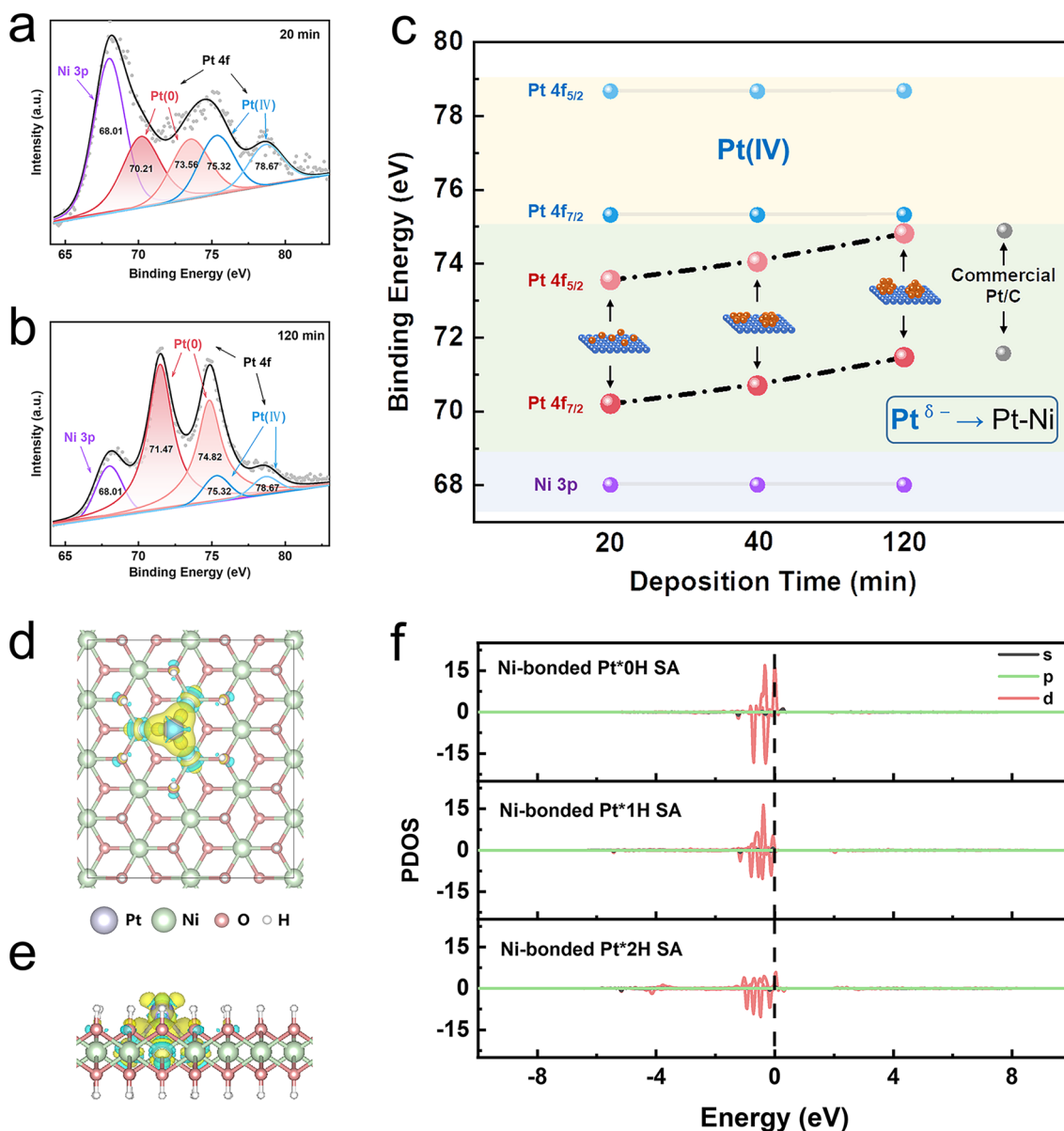


Fig. 3 The negatively charged electronic states of Pt^{δ-} in Pt-SA/a-Ni(OH)₂ catalyst. **a, b** Pt 4*f* XPS spectra of Pt/a-Ni(OH)₂ catalysts with electrodeposition time of 20 and 120 min. **c** Variation of binding energies for Pt/a-Ni(OH)₂ catalysts with different electrodeposition time. **d, e** Charge density differences of Pt SA adsorption on amorphous Ni(OH)₂ with oxygen vacancies from top and side views. Isosurfaces are plotted with 0.003 e Å⁻³. The yellow and blue contours represent electron accumulation and depletion, respectively. **f** Calculated partial density of state (PDOS) of Ni-bonded Pt*0H SA, Ni-bonded Pt*1H SA and Ni-bonded Pt*2H SA with the different number of H atoms, and the corresponding number of H adsorption on Pt are 0, 1, and 2 for Ni-bonded Pt*0H SA, Ni-bonded Pt*1H SA, and Ni-bonded Pt*2H SA, respectively

Pt-SA/a-Ni(OH)₂ with the local environment of Pt–Ni bonding, the Pt atom with greater electron-negative can take electrons from Ni atoms and thus became partially negatively charged. When the electrodeposition time increased, Pt species transforms from SA to particle, and the Pt–Pt bonds take advantages, making its valence state closer to 0 valence.

The novel electronic states of Pt SA were further confirmed by DFT calculations. It demonstrated that when Pt SA was adsorbed onto the Ni(OH)₂ substrate with oxygen vacancies, the three Ni atoms bonded with the Pt SA. As shown in Figs. 3d, e and S9, the charge transfer occurred between Pt SA and the Ni(OH)₂ substrate, resulting in electron gain by the Pt atoms and manifestation of a negatively charged state, aligning with the experimental XPS results. To unravel the underlying mechanisms for the enhanced HER performance within the Pt SA, we conducted a systematic analysis of the electronic structure of the Pt atom under various hydrogen adsorption scenarios on the Pt SA on Ni(OH)₂ substrate (Figs. 3f and S10a). When H adsorption on the Pt–SA, the negative charged Pt donates about 0.11 e to first H atom based on the Bader charge, as shown in Table S2. As discussed above, the Pt behaves as negative charge for the whole process. Thus, the electronic structure of Pt–Ni model is greatly different from the counterpart of Pt–O. As shown in Fig. S10b and Table S3, the Pt of Pt–O system tends to accept a small amount of electrons from Ni(OH)₂ by about –0.03 e. Upon H adsorption, the Pt donates electron to H and Ni(OH)₂, which makes Pt as positive charge (0.28 e). The calculated density of states (DOS) unveiled that upon hydrogen atoms adsorption onto Pt SA, the extra electrons, donated by the Ni(OH)₂ substrate to the Pt SA, could transfer to the hydrogen atoms, thus actively promoting the HER process. Consequently, the Ni-bonded Pt SA structure stands as a catalyst with remarkable efficiency in advancing the HER process.

3.3 HER Mechanisms of Pt–SA/a-Ni(OH)₂ Catalyst

Compared to traditional Pt–O bonded Pt SA, Pt–Ni bonded Pt SA has a lower oxidation state, making them more favorable for adsorption of activated hydrogen atoms in the electrolyte, especially under the alkaline [11, 32]. Compared to the widely studied HER in the acidic, the HER under alkaline conditions has milder reaction conditions and higher energy

conversion efficiency [35, 36]. However, due to the absence of H⁺ in the solution, the water dissociation step of the HER under alkaline medium is slow and the proton supply is poor, making its rate several orders of magnitude lower than that in acidic medium [37–39]. In order to explore the structural advantages of the Pt–SA/a-Ni(OH)₂ catalyst for alkaline HER and the possible reaction mechanisms, the adsorbed species of the catalysts during the catalytic reaction was detected by in situ Raman spectroscopy (Fig. S11). As shown in the Raman spectra of Fig. 4a, there is no Pt–H stretching vibration signal at ~2170 cm⁻¹ before applying voltage [40]. After applying a negative potential for starting HER, a significant Pt–H vibration appeared at ~2170 cm⁻¹, and the intensity of the peak enhanced synchronously with the increase of the applied negative voltage. It demonstrated the strong adsorption capacity and responsivity of hydrogen for the Pt site in Pt–SA/a-Ni(OH)₂, consistent with our speculation that Pt–Ni bonding enhances adsorption for hydrogen atoms.

Apart from Pt–H stretching vibration, another additional peak at ~1630 cm⁻¹ was also observed in Raman spectra when a negative potential was applied. It was attributed to the H–O–H bending vibration [41]. With the increase of the applied negative potential, this peak was also enhanced synchronously, which means that the adsorption of water was also promoted by the catalyst during the HER process. This promotion was also confirmed on pure amorphous Ni(OH)₂ substrate, demonstrating the enhanced adsorption of H₂O molecule on amorphous Ni(OH)₂ (Fig. S12). According to previous report, Ni(OH)₂ can cleave the H–O–H bond of H₂O at the interface of Ni(OH)₂ and Pt, producing hydrogen atoms and transferring them to the active sites for HER reactions [42, 43]. Combined with the synchronously enhanced Pt–H bond, we supposed that amorphous Ni(OH)₂ can accelerate water dissociation process. The generated H_{ad} intermediates transferred to the Pt SA immediately afterward and thus facilitated HER. To validate this hydrogen spillover process, the in situ Raman spectra of commercial Pt/C in HER was also performed (Fig. 4b) [37, 44]. It was found that the H–O–H bending vibrational signal could not be observed at 1630 cm⁻¹, even when a negative voltage was applied. It indicated that compared with amorphous Ni(OH)₂, the adsorption of water molecules is weak for commercial Pt/C. Meanwhile, almost imperceptible Pt–H stretching vibration was exhibited at ~2170 cm⁻¹. It suggested that the amorphous

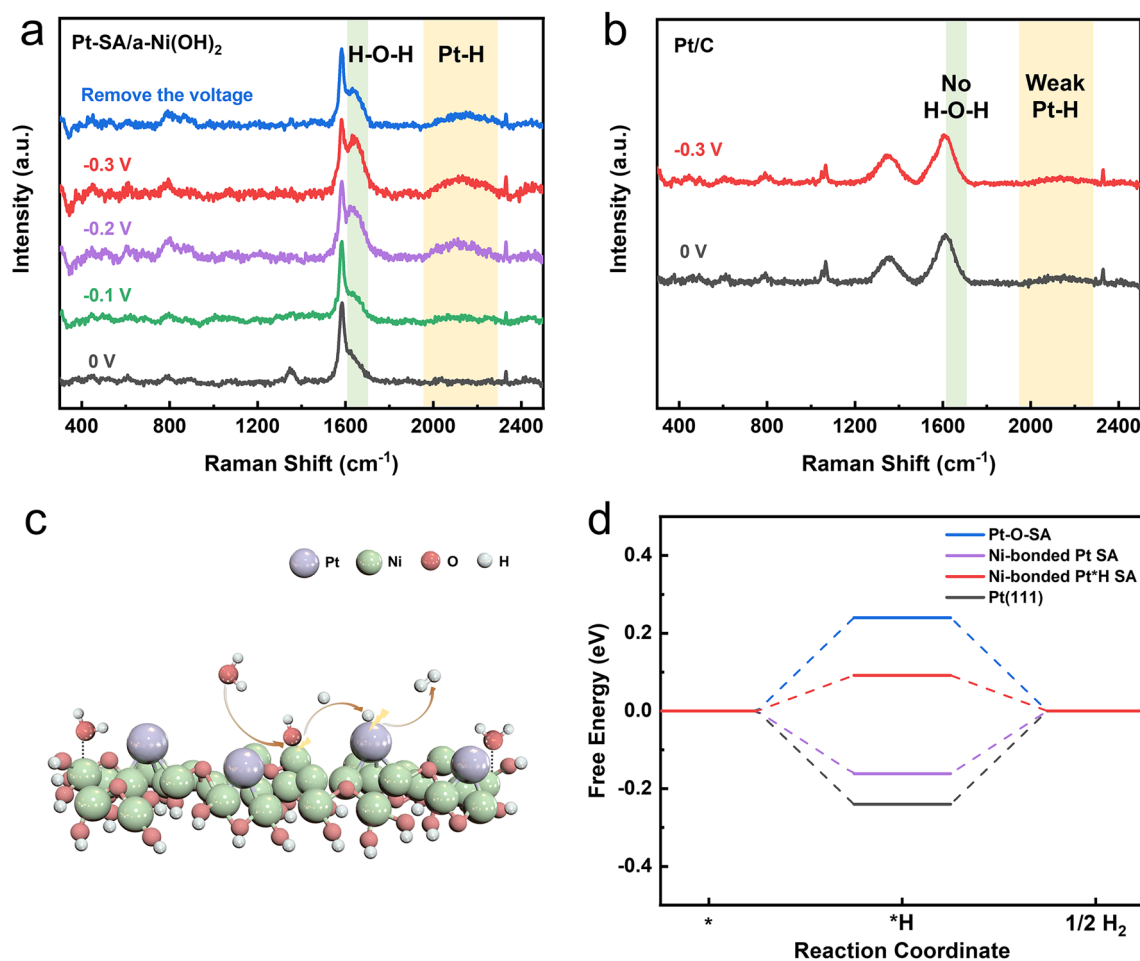


Fig. 4 Strong adsorption capacity of hydrogen for the Pt site in Pt-SA/a-Ni(OH)₂. **a** In situ Raman spectra of Pt-SA/a-Ni(OH)₂ during HER. **b** In situ Raman spectra of commercial Pt/C during HER. **c** Schematic diagram of the hydrogen spillover processes at Pt-SA/a-Ni(OH)₂ during HER. **d** ΔG_{H} of Pt-O-SA, Ni-bonded Pt SA, Ni-bonded Pt*H SA and Pt(111). Pt(111) is regarded as a simplified model for Pt NP in Pt/C

Ni(OH)₂ substrate effectively adsorbed and cleaved water molecules, providing a large number of H_{ad} intermediates for the Pt SA and thus promoting HER (Fig. 4c). Based on the first-principles molecular dynamics (FPMD) simulations, the extra H transfer from Ni(OH)₂ to Pt was observed for 1.73 ps, indicating that H transfer could occur between Ni(OH)₂ and Pt for the model of Pt over Ni atom of Ni(OH)₂, while the H transfer is not observed for the Pt adsorption over the oxygen atom of Ni(OH)₂ for the same FPMD setups (Fig. S13, Movies S1, S2).

DFT calculations were performed to investigate the connection between the material structures and HER performance, and the calculated Gibbs free energy of hydrogen

adsorption (ΔG_{H}) were shown in Fig. 4d. The HER performance could be evaluated by the absolute value of ΔG_{H} , as proposed by by Nørskov [45]. According to the calculated results, compared with the traditional Pt-O based SA catalysts and Pt NP catalysts, Ni-bonded Pt SA shows the lowest ΔG_{H} , indicating the high HER activity (Figs. S14-S16). Furthermore, after the first hydrogen atom has adsorbed on the Pt site, the ΔG_{H} of Ni-bonded Pt*H SA for the next H adsorption process decreases to be as small as 0.09 eV (Fig. S14). Therefore, the Ni-bonded Pt SA catalyst could exhibit an excellent catalytic performance of HER.

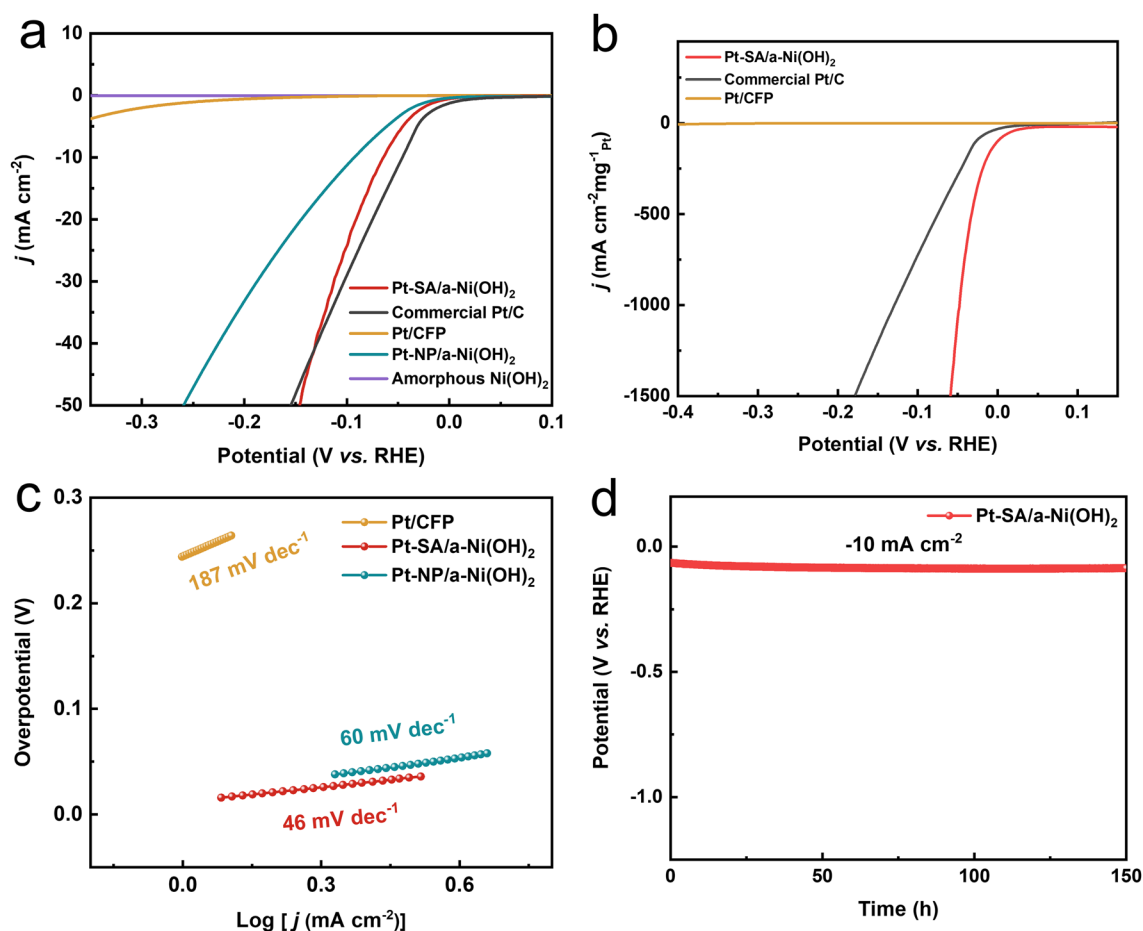


Fig. 5 HER performance of Pt-SA/a-Ni(OH)₂. **a** LSV curves of Pt-SA/a-Ni(OH)₂ catalyst and the comparative samples. **b** Pt normalized LSV curves of Pt-SA/a-Ni(OH)₂ catalyst and commercial Pt/C. **c** Tafel slopes of Pt/CFP, Pt-SA/a-Ni(OH)₂ catalyst, Pt-NP/a-Ni(OH)₂ catalyst. **d** Stability of Pt-SA/a-Ni(OH)₂ evaluated through CA test

3.4 HER Performance of Pt-SA/a-Ni(OH)₂ Catalyst

Then, we quantitatively investigated the alkaline HER performance of Pt-SA/a-Ni(OH)₂ catalyst. Electrochemical tests were performed in a typical three-electrode system in 1 M KOH, employing carbon rod and Hg/HgO electrode as counter and reference electrode. The HER activity of the Pt-SA/a-Ni(OH)₂ catalyst was firstly evaluated by analyzing linear sweep voltammetry (LSV) curves. To reach a current density of -10 mA cm^{-2} in alkaline solution, Pt-SA/a-Ni(OH)₂ catalyst with ultra-low noble metal loading ($\sim 0.07 \text{ wt}\%$) exhibited an overpotential of only 64 mV (Fig. 5a). This overpotential is significantly lower than that of the a-Ni(OH)₂ substrate and the other comparative samples with different types of Pt-based bonds (Figs. 5a and S17), which is also comparable to some recently reported

Pt based works (Table S4) [5, 8, 46–49]. Furthermore, normalized the mass of Pt, its overpotential is only 48 mV at $-1000 \text{ mA cm}^{-2} \text{ mg}^{-1}_{\text{Pt}}$, which is considerably lower than the overpotential of commercial Pt/C of 128 mV (Figs. 5b and S18). The remarkable performance should be attributed to the above mentioned SA of Pt–Ni bonding configuration and its synergistic effect with the amorphous substrates. To confirm the HER mechanism, we conducted the kinetic process of the reaction through calculating the value of Tafel slope (Fig. 5c). The Tafel slope of 46 mV dec^{-1} for Pt-SA/a-Ni(OH)₂ is much lower than those of Pt/CFP and Pt-NP/a-Ni(OH)₂, indicating that the Volmer step of water dissociation in alkaline HER was accelerated in the Pt-SA/a-Ni(OH)₂, in agreement with the Raman spectra results. In addition, the durability of Pt-SA/a-Ni(OH)₂ catalyst was also evaluated through chronoamperometry (CA) test, which

showed that the catalyst kept excellent stability during 150 h of HER (Fig. 5d). The morphology and atomic structure were also well maintained (Fig. S19).

4 Conclusion

In summary, utilizing the exposed Ni sites with oxygen vacancies on amorphous Ni(OH)₂ to anchor Pt, Pt–Ni bonding fixed Pt SA are constructed, instead of Pt–O bonding in the conventional Pt SA catalysts. The novel structure greatly facilitates alkaline HER process by both the unique atomic and electronic structures. The amorphous Ni(OH)₂ substrate effectively adsorbs and cleaves water molecules, accelerating the Volmer step of water dissociation in alkaline HER and providing H_{ad} for the Pt site. Furthermore, the Pt–Ni bond reduces the oxidation state of the Pt SA and thus optimize the adsorption capacity for hydrogen atoms. This work provides a new idea to deeply modulate the configuration of SA catalysts and thus controllably regulate the electronic states of SA catalysts to enhance catalytic performance.

Acknowledgements The authors thank BL11B beamline of the Shanghai Synchrotron Radiation Facility (SSRF) for providing the XAFS beamtime. The work was supported by National Natural Science Foundation of China (52373221, U1910208, 52250119), the National Key R&D Program of China (2020YFA0710403), the Scientific Research Fund of Hunan Provincial Education Department (NO.23B0114).

Declarations

Conflict of interest The authors declare no interest conflict. They have no known competing financial interests or personal relationships that could have appeared to influence the work reported in this paper.

Open Access This article is licensed under a Creative Commons Attribution 4.0 International License, which permits use, sharing, adaptation, distribution and reproduction in any medium or format, as long as you give appropriate credit to the original author(s) and the source, provide a link to the Creative Commons licence, and indicate if changes were made. The images or other third party material in this article are included in the article's Creative Commons licence, unless indicated otherwise in a credit line to the material. If material is not included in the article's Creative Commons licence and your intended use is not permitted by statutory regulation or exceeds the permitted use, you will need to obtain permission directly from the copyright holder. To view a copy of this licence, visit <http://creativecommons.org/licenses/by/4.0/>.

Supplementary Information The online version contains supplementary material available at <https://doi.org/10.1007/s40820-024-01420-6>.

References

1. Y. Hu, T. Chao, Y. Li, P. Liu, T. Zhao et al., Cooperative Ni(Co)–Ru–P Sites activate dehydrogenation for hydrazine oxidation assisting self-powered H₂ production. *Angew. Chem. Int. Ed.* **62**(35), e202308800 (2023). <https://doi.org/10.1002/anie.202308800>
2. J. Park, S. Lee, H. Kim, A. Cho, S. Kim et al., Investigation of the support effect in atomically dispersed Pt on WO_{3-x} for utilization of Pt in the hydrogen evolution reaction. *Angew. Chem. Int. Ed.* **58**(45), 16038–16042 (2019). <https://doi.org/10.1002/anie.201908122>
3. H. Gu, J. Li, X. Niu, J. Lin, L. Chen et al., Symmetry-breaking *p*-block antimony single atoms trigger N-bridged titanium sites for electrocatalytic nitrogen reduction with high efficiency. *ACS Nano* **17**(21), 21838–21849 (2023). <https://doi.org/10.1021/acsnano.3c07857>
4. H. Gu, W. Yue, J. Hu, X. Niu, H. Tang et al., Asymmetrically coordinated Cu–N₁C₂ single-atom catalyst immobilized on Ti₃C₂T_x MXene as separator coating for lithium-sulfur batteries. *Adv. Energy Mater.* **13**(20), 2204014 (2023). <https://doi.org/10.1002/aenm.202204014>
5. Q. Li, Q. Zhang, W. Xu, R. Zhao, M. Jiang et al., Sowing single atom seeds: a versatile strategy for hyper-low noble metal loading to boost hydrogen evolution reaction. *Adv. Energy Mater.* **13**(10), 2203955 (2023). <https://doi.org/10.1002/aenm.202203955>
6. C. Ye, J. Shan, C. Zhu, W. Xu, L. Song et al., Spatial structure engineering of interactive single platinum sites toward enhanced electrocatalytic hydrogen evolution. *Adv. Energy Mater.* **13**(45), 2302190 (2023). <https://doi.org/10.1002/aenm.202302190>
7. C. Wang, L. Kuai, W. Cao, H. Singh, A. Zakharov et al., Highly dispersed Cu atoms in MOF-derived N-doped porous carbon inducing Pt loads for superior oxygen reduction and hydrogen evolution. *Chem. Eng. J.* **426**(15), 130749 (2021). <https://doi.org/10.1016/j.cej.2021.130749>
8. Z. Chen, X. Li, J. Zhao, S. Zhang, J. Wang et al., Stabilizing Pt single atoms through Pt–Se electron bridges on vacancy-enriched nickel selenide for efficient electrocatalytic hydrogen evolution. *Angew. Chem. Int. Ed.* **62**(39), e202308686 (2023). <https://doi.org/10.1002/anie.202308686>
9. R. Li, D. Wu, P. Rao, P. Deng, J. Li et al., General approach for atomically dispersed precious metal catalysts toward hydrogen reaction. *Carbon Energy* **5**(7), e294 (2023). <https://doi.org/10.1002/cey2.294>
10. K. Chen, N. Zhang, F. Wang, J. Kang, K. Chu, Main-group indium single-atom catalysts for electrocatalytic NO reduction

- to NH_3 . *J. Mater. Chem. A* **11**(13), 6814–6819 (2023). <https://doi.org/10.1039/d3ta00606a>
11. X. Cheng, B. Xiao, Y. Chen, Y. Wang, L. Zheng et al., Ligand charge donation-acquisition balance: a unique strategy to boost single Pt atom catalyst mass activity toward the hydrogen evolution reaction. *ACS Catal.* **12**(10), 5970–5978 (2022). <https://doi.org/10.1021/acscatal.2c00891>
 12. P. Kuang, Y. Wang, B. Zhu, F. Xia, C. Tung et al., Pt single atoms supported on N-doped mesoporous hollow carbon spheres with enhanced electrocatalytic H_2 -evolution activity. *Adv. Mater.* **33**(18), 2008599 (2021). <https://doi.org/10.1002/adma.202008599>
 13. H. Yang, Y. Ji, Q. Shao, W. Zhu, M. Fang et al., Metastable-phase platinum oxide for clarifying the Pt–O active site for the hydrogen evolution reaction. *Energy Environ. Sci.* **16**(2), 574–583 (2023). <https://doi.org/10.1039/D2EE03351H>
 14. W. Chen, Y. Ma, F. Li, L. Pan, W. Gao et al., Strong electronic interaction of amorphous Fe_2O_3 nanosheets with single-atom Pt toward enhanced carbon monoxide oxidation. *Adv. Funct. Mater.* **29**(42), 1904278 (2019). <https://doi.org/10.1002/adfm.201904278>
 15. Q. Fu, L. Wong, F. Zheng, X. Zheng, C.S. Tsang et al., Unraveling and leveraging in situ surface amorphization for enhanced hydrogen evolution reaction in alkaline media. *Nat. Commun.* **14**(1), 6462 (2023). <https://doi.org/10.1038/s41467-023-42221-6>
 16. J. Nai, H. Yin, T. You, L. Zheng, J. Zhang et al., Efficient electrocatalytic water oxidation by using amorphous Ni–Co double hydroxides nanocages. *Adv. Energy Mater.* **5**(10), 1401880 (2015). <https://doi.org/10.1002/aenm.201401880>
 17. X. Chen, S. Lv, J. Kang, Z. Wang, T. Guo et al., Efficient C–N coupling in the direct synthesis of urea from CO_2 and N_2 by amorphous $\text{Sb}_x\text{Bi}_{1-x}\text{O}_y$ clusters. *Proc. Natl. Acad. Sci. U.S.A.* **120**(39), e2306841120 (2023). <https://doi.org/10.1073/pnas.2306841120>
 18. J. Kang, X. Chen, R. Si, X. Gao, S. Zhang et al., Activating Bi *p*-orbitals in dispersed clusters of amorphous BiO_x for electrocatalytic nitrogen reduction. *Angew. Chem. Int. Ed.* **62**(15), e202217428 (2023). <https://doi.org/10.1002/anie.202217428>
 19. Y. Zhao, Z. Huang, L. Wang, X. Chen, Y. Zhang et al., Highly efficient and recyclable amorphous Pd(II)/crystal Pd(0) catalyst for boosting Suzuki reaction in aqueous solution. *Nano Res.* **15**(2), 1193–1198 (2022). <https://doi.org/10.1007/s12274-021-3623-5>
 20. J. Du, Y. Huang, Z. Huang, G. Wu, B. Wu et al., Reversing the catalytic selectivity of single-atom Ru via support amorphization. *JACS Au* **2**(5), 1078–1083 (2022). <https://doi.org/10.1021/jacsau.2c00192>
 21. Y. Liu, X. Liu, A.R. Jadhav, T. Yang, Y. Hwang et al., Unraveling the function of metal-amorphous support interactions in single-atom electrocatalytic hydrogen evolution. *Angew. Chem. Int. Ed.* **61**(9), e202114160 (2022). <https://doi.org/10.1002/anie.202114160>
 22. D. Feng, P. Wang, R. Qin, W. Shi, L. Gong et al., Flower-like amorphous MoO_{3-x} stabilized Ru single atoms for efficient overall water/seawater splitting. *Adv. Sci.* **10**(18), 2300342 (2023). <https://doi.org/10.1002/advs.202300342>
 23. Y. Hu, G. Luo, L. Wang, X. Liu, Y. Qu et al., Single Ru atoms stabilized by hybrid amorphous/crystalline FeCoNi layered double hydroxide for ultraefficient oxygen evolution. *Adv. Energy Mater.* **11**(1), 2002816 (2021). <https://doi.org/10.1002/aenm.202002816>
 24. K. Chen, Y. Zhang, J. Xiang, X. Zhao, X. Li et al., *p*-Block antimony single-atom catalysts for nitric oxide electroreduction to ammonia. *ACS Energy Lett.* **8**(3), 1281–1288 (2023). <https://doi.org/10.1021/acscenergylett.2c02882>
 25. L. Zeng, Z. Zhao, Q. Huang, C. Zhou, W. Chen et al., Single-atom Cr– N_4 sites with high oxophilicity interfaced with Pt atomic clusters for practical alkaline hydrogen evolution catalysis. *J. Am. Chem. Soc.* **145**(39), 21432–21441 (2023). <https://doi.org/10.1021/jacs.3c06863>
 26. J. Kang, Y. Xue, J. Yang, Q. Hu, Q. Zhang et al., Realizing two-electron transfer in $\text{Ni}(\text{OH})_2$ nanosheets for energy storage. *J. Am. Chem. Soc.* **144**(20), 8969–8976 (2022). <https://doi.org/10.1021/jacs.1c13523>
 27. J. Kang, X. Qiu, Q. Hu, J. Zhong, X. Gao et al., Valence oscillation and dynamic active sites in monolayer NiCo hydroxides for water oxidation. *Nat. Catal.* **4**(12), 1050–1058 (2021). <https://doi.org/10.1038/s41929-021-00715-w>
 28. J. Kang, G. Liu, Q. Hu, Y. Huang, L.M. Liu et al., Parallel nanosheet arrays for industrial oxygen production. *J. Am. Chem. Soc.* **145**(46), 25143–25149 (2023). <https://doi.org/10.1021/jacs.3c05688>
 29. W. Guo, X. Gao, M. Zhu, C. Xu, X. Zhu et al., A closely packed $\text{Pt}_{1.5}\text{Ni}_{1-x}/\text{Ni}-\text{N}-\text{C}$ hybrid for relay catalysis towards oxygen reduction. *Energy Environ. Sci.* **16**(1), 148–156 (2023). <https://doi.org/10.1039/D2EE02381D>
 30. M. Wang, Y. Xu, C.K. Peng, S.Y. Chen, Y.G. Lin et al., Site-specified two-dimensional heterojunction of Pt nanoparticles/metal-organic frameworks for enhanced hydrogen evolution. *J. Am. Chem. Soc.* **143**(40), 16512–16518 (2021). <https://doi.org/10.1021/jacs.1c06006>
 31. T. Zhang, Z. Zhao, D. Zhang, X. Liu, P. Wang et al., Superexchange-induced Pt–O– Ti^{3+} site on single photocatalyst for efficient H_2 production with organics degradation in wastewater. *Proc. Natl. Acad. Sci. U.S.A.* **120**(23), e2302873120 (2023). <https://doi.org/10.1073/pnas.2302873120>
 32. Y. Li, A.I. Frenkel, Deciphering the local environment of single-atom catalysts with X-ray absorption spectroscopy. *Acc. Chem. Res.* **54**(11), 2660–2669 (2021). <https://doi.org/10.1021/acs.accounts.1c00180>
 33. M. Zhou, H. Li, A. Long, B. Zhou, F. Lu et al., Modulating 3D orbitals of Ni atoms on Ni–Pt edge sites enables highly-efficient alkaline hydrogen evolution. *Adv. Energy Mater.* **11**(36), 2101789 (2021). <https://doi.org/10.1002/aenm.202101789>
 34. K. Zhou, Z. Wang, C. Han, X. Ke, C. Wang et al., Platinum single-atom catalyst coupled with transition metal/metal oxide heterostructure for accelerating alkaline hydrogen evolution reaction. *Nat. Commun.* **12**(1), 3783 (2021). <https://doi.org/10.1038/s41467-021-24079-8>



35. X. Xiao, Z. Li, Y. Xiong, Y.W. Yang, IrMo nanocluster-doped porous carbon electrocatalysts derived from cucurbit[6]uril boost efficient alkaline hydrogen evolution. *J. Am. Chem. Soc.* **145**(30), 16548–16556 (2023). <https://doi.org/10.1021/jacs.3c03489>
36. X. Liu, Y. Jiang, J. Huang, W. Zhong, B. He et al., Bifunctional PdPt bimetallics for formate oxidation-boosted water electrolysis. *Carbon Energy* **5**(12), e367 (2023). <https://doi.org/10.1002/cey2.367>
37. J. Chen, C. Chen, M. Qin, B. Li, B. Lin et al., Reversible hydrogen spillover in Ru–WO_{3-x} enhances hydrogen evolution activity in neutral pH water splitting. *Nat. Commun.* **13**(1), 5382 (2022). <https://doi.org/10.1038/s41467-022-33007-3>
38. X. Chen, X.T. Wang, J.B. Le, S.M. Li, X. Wang et al., Revealing the role of interfacial water and key intermediates at ruthenium surfaces in the alkaline hydrogen evolution reaction. *Nat. Commun.* **14**(1), 5289 (2023). <https://doi.org/10.1038/s41467-023-41030-1>
39. C. Wan, Z. Zhang, J. Dong, M. Xu, H. Pu et al., Amorphous nickel hydroxide shell tailors local chemical environment on platinum surface for alkaline hydrogen evolution reaction. *Nat. Mater.* **22**(8), 1022–1029 (2023). <https://doi.org/10.1038/s41563-023-01584-3>
40. X. Wang, C. Xu, M. Jaroniec, Y. Zheng, S.Z. Qiao, Anomalous hydrogen evolution behavior in high-pH environment induced by locally generated hydronium ions. *Nat. Commun.* **10**(1), 4876 (2019). <https://doi.org/10.1038/s41467-019-12773-7>
41. T. Zhang, J. Jin, J. Chen, Y. Fang, X. Han et al., Pinpointing the axial ligand effect on platinum single-atom-catalyst towards efficient alkaline hydrogen evolution reaction. *Nat. Commun.* **13**(1), 6875 (2022). <https://doi.org/10.1038/s41467-022-34619-5>
42. R. Subbaraman, D. Tripkovic, D. Strmcnik, K.C. Chang, M. Uchimura et al., Enhancing hydrogen evolution activity in water splitting by tailoring Li⁺–Ni(OH)₂–Pt interfaces. *Science* **334**(6060), 1256–1260 (2011). <https://doi.org/10.1126/science.1211934>
43. Q. Xu, Heterogeneous interface engineered atomic configuration on ultrathin Ni(OH)₂/Ni₃S₂ nanoforests for efficient water splitting. *Appl. Catal. B* **242**, 60–66 (2019). <https://doi.org/10.1016/j.apcatb.2018.09.064>
44. A. Mahdavi-Shakib, T.N. Whittaker, T.Y. Yun, K.B. Srajan Kumar, L.C. Rich et al., The role of surface hydroxyls in the entropy-driven adsorption and spillover of H₂ on Au/TiO₂ catalysts. *Nat. Catal.* **6**(1), 710–719 (2023). <https://doi.org/10.1038/s41929-023-00996-3>
45. J.K. Nørskov, T. Bligaard, A. Logadottir, J.R. Kitchin, J.G. Chen et al., Trends in the exchange current for hydrogen evolution. *J. Electrochem. Soc.* **152**(3), J23 (2005). <https://doi.org/10.1149/1.1856988>
46. Q. Yang, H. Liu, P. Yuan, Y. Jia, L. Zhuang et al., Single carbon vacancy traps atomic platinum for hydrogen evolution catalysis. *J. Am. Chem. Soc.* **144**(5), 2171–2178 (2022). <https://doi.org/10.1021/jacs.1c10814>
47. H. Zhang, P. An, W. Zhou, B. Guan, P. Zhang et al., Dynamic traction of lattice-confined platinum atoms into mesoporous carbon matrix for hydrogen evolution reaction. *Sci. Adv.* **4**(1), eaao6657 (2018). <https://doi.org/10.1126/sciadv.aao6657>
48. Y. Tian, M. Wen, A. Huang, Q. Wu, Z. Wang et al., Significantly stabilizing hydrogen evolution reaction induced by Nb-doping Pt/Co(OH)₂ nanosheets. *Small* **19**(20), 2207569 (2023). <https://doi.org/10.1002/sml.202207569>
49. X. Wan, H. Wu, B. Guan, D. Luan, X. Lou, Confining subnanometer Pt clusters in hollow mesoporous carbon spheres for boosting hydrogen evolution activity. *Adv. Mater.* **32**(7), 1901349 (2020). <https://doi.org/10.1002/adma.201901349>